An experimental and theoretical investigation of phonons and lattice instabilities in metastable decompressed $SrGeO_3$ perovskite

1998 J. Phys.: Condens. Matter 10 221

(http://iopscience.iop.org/0953-8984/10/1/025)

J. Phys.: Condens. Matter **10** (1998) 221–233. Printed in the UK PII: S0953-8984(98)83913-1

An experimental and theoretical investigation of phonons and lattice instabilities in metastable decompressed $SrGeO_3$ perovskite

A Grzechnik†‡, A V G Chizmeshya†, G H Wolf† and P F McMillan†

† Department of Chemistry, Arizona State University, Tempe, AZ 85287-1604, USA

‡ Ecole Normale Supérieure de Lyon, 46 allée d'Italie, 69364 Lyon Cédex 07, France

Received 1 May 1997, in final form 16 September 1997

Abstract. We report detailed Raman and IR spectroscopic measurements for the decompressed high-pressure perovskite phase of $SrGeO_3$. The appearance of a first-order Raman spectrum and slight splittings in the infrared bands suggest that the symmetry of the recovered metastable perovskite phase is lowered from $Pm3m$. This interpretation is fully supported by first-principles LDA calculations using the LAPW method, which indicate a small tetragonal distortion. The static lattice energy is lowered by 3.3 meV (per formula unit) by allowing rotational relaxation of the GeO_6 octahedra. The calculations permit a reliable assignment of the zone centre phonon modes of $SrGeO_3$ perovskite. The calculated pressure dependence of the ferroic IR-active modes is in excellent agreement with our measured data and reveals an incipient soft-mode behaviour in the tension regime. Further calculations of the GeO_6 unit as a function of octahedral volume reveal instabilities to local off-centre Ge^{4+} displacements as the octahedra are expanded. This provides a detailed understanding of the large dielectric constant ($e(0) \sim 100$) for this non-transition-metal-containing decompressed perovskite phase.

1. Introduction

There has been much interest concerning the transformation of silicate and germanate materials ($ASiO_3$, $AGeO_3$: $A = Mg, Ca, Sr,$ etc) to perovskite and perovskite-related structures at high pressure. The low-pressure forms of these materials are tetrahedral (GeO_3^{2-}, SiO_3^{2-}) chain structures. Decompressed perovskite phases exhibit an interesting display of elastic and phonon instabilities, which result in spontaneous transformation to amorphous or metastable crystalline forms at or near ambient temperature. These instabilities also confer potentially interesting materials properties, including high dielectric and possibly ferroelectric-like behaviour, on the recovered metastable perovskites.

The principal compounds of interest include $MgSiO_3$, $MgGeO_3$, $CaGeO_3$, $CaSiO_3$ [1] and $SrGeO_3$ [2], which all transform to the perovskite phase at high pressure. $MgSiO_3$ is stable in a non-polar orthorhombic perovskite structure above 23 GPa [1, 2]. It can be metastably quenched to ambient pressure in this form, but, upon heating to only 423 K at atmospheric pressure, it transforms to an amorphous phase with silicon in tetrahedral coordination [3]. $MgGeO_3$ forms an orthorhombic polymorph of perovskite at room temperature and 12–14 GPa by pressure-induced phase transition from its lithium niobate form [4]. This transition is fully reversible on decompression. $CaGeO_3$ transforms to orthorhombic perovskite near 6.5 GPa [5]. The high-temperature stability limit of the metastable perovskite phase at ambient pressure lies near 823 K, where a transformation is

0953-8984/98/010221+13$19.50

observed to an amorphous phase with germanium in tetrahedral coordination [6]. Far-infrared spectroscopy of $CaGeO_3$ at high pressure showed that there is no soft-mode behaviour along the decompression route [7].

$CaSiO_3$ crystallizes in the cubic perovskite structure above 10 GPa [8] and then, on decompression, it decays completely to an amorphous phase within a few hours or days at room temperature [9]. We have recently investigated the instability and crystalline–amorphous (C $\rightarrow$ A) transition in $CaSiO_3$ perovskite near ambient pressure using a combination of molecular dynamics and *ab initio* lattice dynamics studies [10, 11]. Our results indicate that the C $\rightarrow$ A transition is triggered by a soft ferroic transverse optic mode, in which the atomic displacements involve out-of-phase oscillations of the Ca and Si atoms. This work suggests that interesting ferroic behaviour might be encountered in other decompressed perovskite materials, with sufficient stability to resist amorphization at ambient conditions.

In this study we report the structure and metastability of the decompressed high-pressure perovskite phase of $SrGeO_3$. The experimentally observed features are rationalized by first-principles calculations using the LAPW method. We have carried out a detailed theoretical calculation of the equation of state of cubic $SrGeO_3$ perovskite, using density-functional theory (DFT) within the local density approximation (LDA). We have also investigated the volume dependence of the infrared active TO modes in $SrGeO_3$ perovskite using the frozen optic phonon method. The role of zone-edge instabilities in the $SrGeO_3$ system was explored by calculating explicitly the variations of the static lattice energy with respect to octahedral tilts and rotations, and the local instability of the GeO_6 units as a function of octahedral volume. This combined experimental and theoretical approach may provide new insight into the behaviour of metastable decompressed $SrGeO_3$ perovskite and related perovskite materials obtained by a high-pressure synthesis route.

2. Experimental procedures

The $SrGeO_3$ pseudowollastonite phase was obtained from a stoichiometric mixture of $SrCO_3$ and GeO_2, heated at 1323 K for 2 days. Synthesis of the perovskite form at 7 GPa and 1373 K was carried out using a Walker-type split-cylinder multianvil apparatus [12].

The IR reflectance spectra from compressed pellets of powder samples were collected with a Biorad Digilab FTS-40 equipped with a specular reflectance device in the range 700–40 cm^{-1} at the main bench of the FTIR instrument (a 12.5 μm Mylar beamsplitter, deuterated tryglycine sulphate detector and a mercury arc source) and the Biorad Digilab UMA–300 microscope attachment in the 4000–450 cm^{-1} range (a KBr beamsplitter, mercury–cadmium–tellurium detector and a ceramic globar source). Details of the infrared reflectivity measurements from powder samples are discussed in [13].

In the high-pressure infrared absorbance experiments in the range 4000–450 cm^{-1} at the main bench of the spectrometer (KBr beamsplitter, HgCdTe detector and ceramic globar source) a sample of $SrGeO_3$ perovskite, with CsI as a pressure medium, was loaded into a Mao–Bell-type cell with type II-a diamonds, brilliant cut with 600 mm culets, and a sample chamber diameter of 250 mm. Pressures were determined from the shift of the R_1 ruby fluorescence line using the scale by Mao *et al* [14].

Raman spectra were measured in backscattering geometry with an ISA S-3000 triple spectrograph with CCD detection (a Princeton Instruments LN/CCD-1100 detector). The laser focusing and signal collection optics systems were built around a modified BH-2 Olympus microscope. The scattered signal was focused and spatially filtered on the entrance slit of the spectrometers. Raman scattering was excited using the 488.0 nm line of an Ar^+

ion laser (Coherent model 90-5). Low- and high-temperature measurements were conducted using a Linkam 600 TH stage.

Dielectric measurements at 100 Hz were carried out on compressed, gold-sputtered, powder samples using a 3314A function generator (Hewlett–Packard), 5210 lock-in amplifier (Princeton Applied Research) and 1615-A capacitance bridge (General Radio Company).

3. Theoretical procedures and equation of state of $SrGeO_3$ perovskite

The relativistic Kohn–Sham equations were solved self-consistently using the full-potential linearized augmented plane wave (FLAPW) method [15]. The static lattice equation of state (EOS) for the cubic phase of $SrGeO_3$ was obtained by calculating the Kohn–Sham [16] ground state energy as a function of volume. This quantity, denoted $U(V)$, was computed at twelve equally spaced volumes ranging from 60 to 40 Å^3. Fixed 'muffin-tin' radius ratios were used to scale the plane-wave part of the calculation in a way that ensured consistent energy convergence at each volume. The parameter RK_{max}, which is the product of the largest plane-wave (cutoff) wavevector and the smallest 'muffin-tin' sphere, is a rough measure of the quality of the basis used to expand the crystalline wavefunctions [11]. Equation of state parameters were obtained by fitting the computed $U(V)$ points to a third-order Birch–Murnaghan state equation. The free parameters in the fit are the ambient pressure values of the unit cell volume V_0, the internal energy E_0 and the bulk modulus K_0 and its pressure derivative K_0'. The convergence of the EOS parameters with respect to RK_{max} is demonstrated in table 1. An examination of the trends reveals that convergence is essentially achieved for $RK_{max} = 8$. It should be noted that while an $RK_{max} = 9$ calculation yields marginal improvement in the calculated EOS properties (typically less than 0.1% for any given parameter) it is much more computationally expensive.

Table 1. Convergence of equation of state properties. Each set of parameters was obtained from a fit of twelve calculated $E(V)$ points to a third-order Birch–Murnaghan equation of state. Volumes are quoted in cubic ångströms; bulk moduli are in GPa and energies are given in Hartrees (atomic units: 1 Hartree = 27.212 eV). Experimental values were taken from Sato and Akimoto [19].

RK_{max}	V_0	K_0	K_0'	E_0
Static lattice				
6	59.15	156.15	4.45	−1.119 166
7	55.51	179.80	4.55	−1.255 160
8	54.57	185.56	4.69	−1.290 000
9	54.43	186.76	4.67	−1.296 985
300 K corrected				
6	59.99	145.19	4.62	−1.106 317
7	56.17	169.80	4.73	−1.240 514
8	55.20	175.75	4.86	−1.274 906
9	55.05	176.95	4.85	−1.281 818
Experiment	55.5	189	4.8	

In order to make a meaningful comparison with available experimental EOS data we have taken into account the effect of thermal expansion to 300 K by combining the volume dependence of the thermal (vibrational) free energy, $F_{th}(V)$, and the internal energy of the static crystal [17]. To estimate the volume dependence of the vibrational free energy we carried out a series of non-empirical lattice dynamical calculations using the variationally

induced breathing (VIB) model [18]. Electron-gas-based LDA estimates for the kinetic and exchange–correlation effects are used to compute the dynamical interactions in a crystal model consisting of overlapping, and deformable, Kohn–Sham ions. The 300 K thermal free energy was computed at the same volume points as in the LAPW runs, and the resulting $F_{th}(V)$ points were fitted to a fourth-order polynomial in volume (see table 2). The internal energy of the thermal crystal at 300 K was then constructed as $E_{th}(V) = U(V) + F_{th}(V)$ and re-fitted to the Birch–Murnagham equation of state.

Table 2. Polynomial fit coefficients of the thermal free energy volume dependence. Superscripts$^{(n)}$ denote the coefficients of the V_n terms.

$F_{th}^{(0)}$ (H)	$F_{th}^{(1)}$ (H Å^3)	$F_{th}^{(2)}$ (H Å^6)	$F_{th}^{(3)}$ (H Å^9)	$F_{th}^{(4)}$ (H Å^{12})
$4.763\,77 \times 10^{-1}$	-3.2411×10^{-2}	$8.773\,85 \times 10^{-4}$	-1.06891×10^{-5}	$4.869\,47 \times 10^{-8}$

The thermal equation of state parameters obtained from this prescription are listed in table 1, which also contains the corresponding experimental estimates of Sato and Akimoto [19]. While the thermally corrected LAPW estimates for the numerical values of V_0, K_0 and K_0' are evidently in very good agreement with the data, it should be noted that the experimental values were deduced from a very limited $P(V)$ data set extending only to about 10 GPa (5% volume compression) (figure 1).

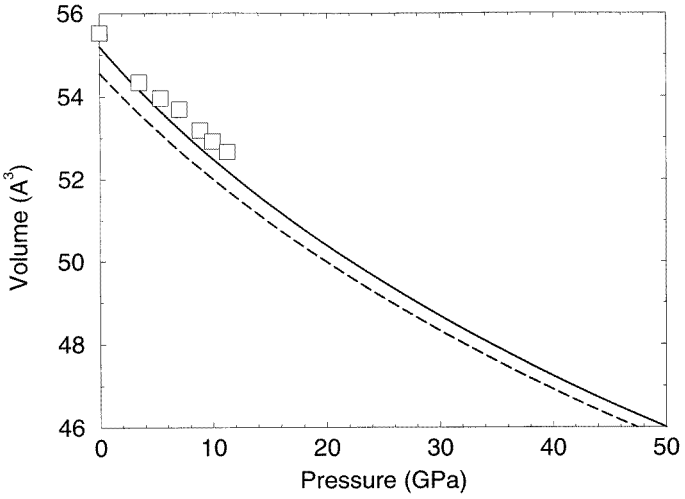

Figure 1. Equation of state of $SrGeO_3$ to 50 GPa. The open squares are the data of [19]; solid line, thermally corrected FLAPW calculation; dashed line, static lattice FLAPW calculation.

4. Results and discussion

The stable form of $SrGeO_3$ at ambient pressure is a pseudowollastonite structure with fourfold-coordinated germanium atoms in metagermanate GeO_3^{2-} chains aligned along the *c* axis. $SrGeO_3$ pseudowollastonite transforms to a distorted garnet form (the Ge atoms are both four and sixfold coordinated) above 1 GPa, and finally to perovskite above 5 GPa at

temperatures in the range 1073–1273 K [19–21]. The x-ray powder patterns of $SrGeO_3$ perovskite samples recovered from different synthesis runs at 7 GPa and 1373 K in this study showed only reflections for the ideal cubic perovskite phase ($Pm3m$ space group), in agreement with the previous reports [13, 19–23].

The ideal cubic structure of ABO_3 perovskite ($Pm3m$ space group) is comprised of corner-shared BO_6 octahedra located at the corners of a cube around a central A atom in a twelvefold (AO_{12}) coordination. Phase transformations observed in perovskites can be described in terms of soft-mode lattice instabilities at the centre or boundaries of the cubic Brillouin zone (the ferroelectric and anti-ferrodistortive transitions, respectively). In the case of the ferroelectric transformations, the A and B cation sublattices are displaced along the c axis, relative to the oxygen sublattice, to remove the centre of inversion in the ideal cubic structure ($Pm3m \rightarrow P4mm$). On the other hand, the cooperative rotations of the BO_6 octahedra at the R (the *out-of-phase* rotations of the octahedra about the c axis: $Pm3m \rightarrow I4/mcm$) and M (the *in-phase* rotations of the BO_6 octahedra about the c axis: $Pm3m \rightarrow P4/mbm$) points of the cubic Brillouin zone lead to antiferrodistortive phase transitions. In general, the combined effect of these distortions gives rise to a wide range of cubic, tetragonal, orthorhombic and rhombohedral structures. Their sequence and systematics have been described extensively in the literature [24–30].

Analysis of the optically active modes in cubic ABO_3 perovskite at the centre of the Brillouin zone shows that first-order Raman scattering is forbidden by symmetry, and that the infrared spectrum should exhibit three modes, $3F_{1u}$. It has been pointed out [31] that the atomic displacement patterns of the lowest-frequency mode in the infrared spectra of cubic oxide perovskites with transition element at the B site consist predominantly of the B cation oscillations within the oxygen cages. The lowered frequency of these modes is due to their strong coupling with the higher-frequency BO_6 bending modes. In the case of non-transition metal perovskites, in which this coupling is weaker, the lowest-frequency mode is usually assigned to the vibrations of the A cations against the BO_6 octahedra [31]. Any features observed in the Raman spectra of cubic perovskites are usually assigned to second-order Raman scattering with wave vectors at or near the cubic Brillouin zone boundary [32–34]. The details of group theoretical considerations for ideal and distorted perovskite structures are given in [25], [27] and [28]. In general, lowered symmetry of the perovskite lattice leads to the appearance of first-order Raman scattering and an increased number of infrared-active modes.

Raman spectra of $SrGeO_3$ perovskite obtained in this study, collected over the temperature range 93–673 K, are shown in figure 2. The spectrum at ambient conditions exhibits several sharp peaks, at 95, 225, 509 and 780 cm^{-1}, which do not resemble the broad second-order features observed in cubic perovskites [32–34]. Upon cooling to liquid nitrogen temperature, these four bands sharpen slightly, and their intensities follow Bose–Einstein statistics consistent with a *first*-order Raman spectrum [35]. Their presence in the Raman spectrum of $SrGeO_3$ perovskite indicates a slight distortion from the ideal cubic lattice, not revealed by the x-ray powder diffraction results. This observation is consistent with our theoretical results, described below. There is no evidence of any soft-mode behaviour in the Raman data.

When $SrGeO_3$ perovskite is externally heated, its crystalline structure completely breaks down by 673 K (figure 2). However, the onset of the structural degradation is observed as low as 398 K, where a strong peak appears at 820 cm^{-1}, due to the tetrahedral Ge–O vibration of the garnet phase (which contains Ge in both tetrahedral and octahedral sites). Broad bands at about 250 and 500 cm^{-1} also appear in this 'intermediate' range of structural breakdown, and could correspond to vibrations of a highly disordered garnet phase, or to

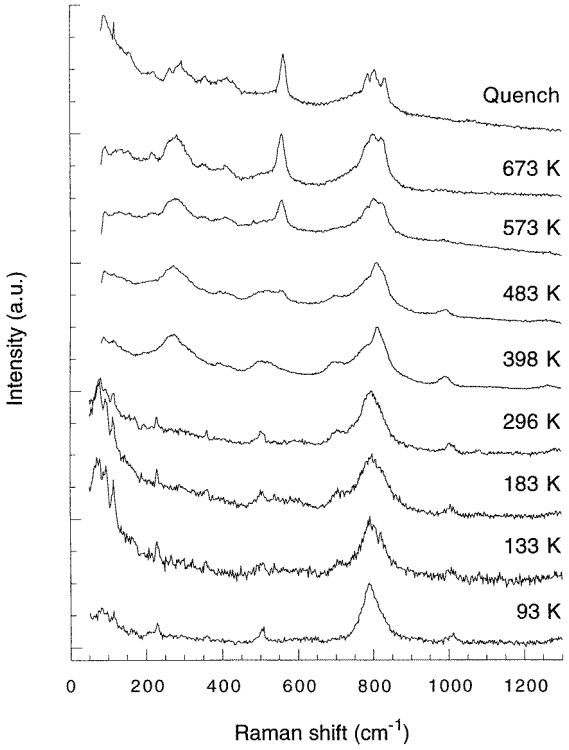

Figure 2. Temperature dependence of the Raman spectrum of $SrGeO_3$, taken at ambient pressure. The spectrum marked 'Quench' was obtained at room temperature after cycling to 673 K.

some other material in the partially transformed sample. Above 483 K, a new peak is observed near 590 cm^{-1}, which eventually dominates the spectrum. At the same time, additional structure is observed in the Ge–O stretching region, near 800 cm^{-1} (figure 2). These are assigned to Ge–O–Ge bending and GeO_4 stretching modes in the tetrahedral chain or ring structure of a wollastonite-type phase. Our experiments are in essential agreement with previous XANES/XAFS studies of this decompressed perovskite material [22, 23], which indicated that high-temperature transformations in $SrGeO_3$ perovskite occur *via* (at least) a two-step mechanism. These authors suggested the formation of an 'amorphous' phase with octahedrally coordinated Ge atoms between 373 and 473 K and a subsequent transformation into fourfold-coordinated amorphous and crystalline phases. It is also possible that the intermediate 'amorphous' phase contains or corresponds to poorly crystalline garnet, as suggested by the Raman results.

Representative infrared reflectance spectra of powdered samples of $SrGeO_3$ perovskite in the 40–1400 cm^{-1} IR region at ambient pressure and temperature are shown in figure 3. Some variation in these spectra was noted from one synthesis run to another, related to the underlying lattice metastability discussed here. All of the IR spectra show three principal modes ($3F_{1u}$), as expected from symmetry analysis for the ideal cubic perovskite lattice. However, the structure observed on the three main bands indicates deviations from cubic symmetry, in agreement with the observation of first-order Raman scattering (figure 2). In order to carry out an analysis of the infrared reflectivity data, we used a factorized form

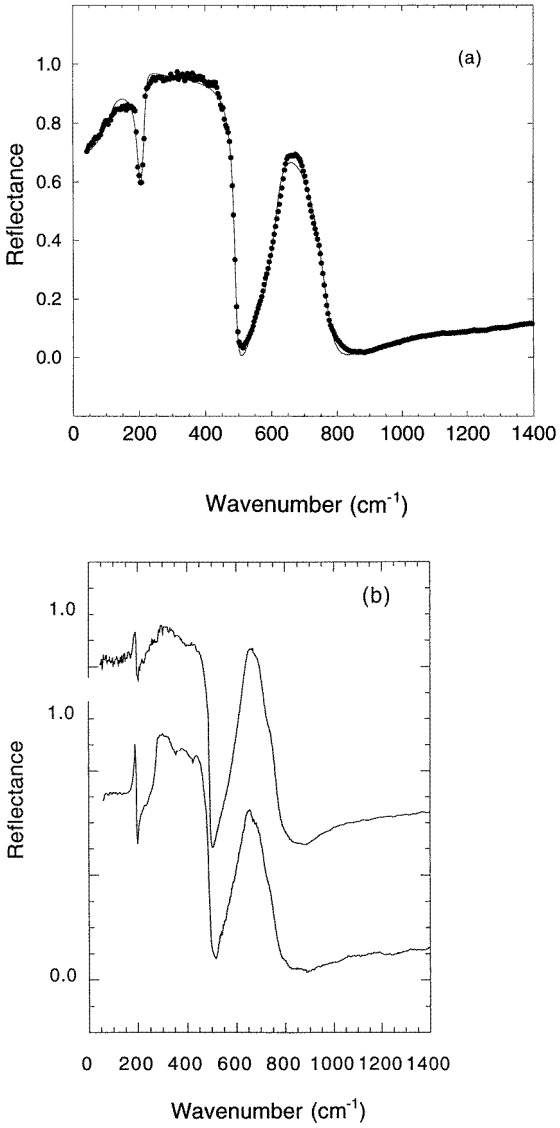

Figure 3. Infrared reflectance spectra (taken at room temperature) of different samples of $SrGeO_3$ perovskite recovered from different synthesis runs in multianvil. (a) Points represent the measured spectrum; solid line is the calculated spectrum obtained from a dielectric function fit. (b) Band splittings (lower trace) due to slight non-cubic structural distortion.

of the dielectric response function to extract the optical parameters [36]. The results of empirical fitting of that function to the IR spectra are shown in figure 3 (solid lines), and the numerical results for a typical fit (figure 3(a)) are given in table 3. As can be seen, the oscillator strength of the lowest-frequency mode at 120 cm^{-1} provides the dominant contribution to the static dielectric constant ($\varepsilon(0) = 114$). This value is typical for cubic perovskites with a transition metal at the B site [13, 36, 37]. The presence of the 'spike' near 200 cm^{-1} in figure 3(b) requires the presence of an additional weak oscillator in the

fit.

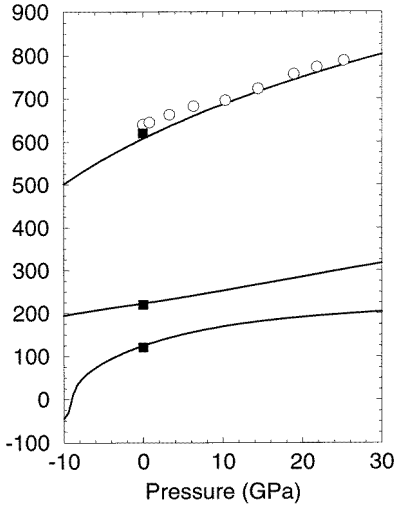

Figure 4. Pressure dependence of the transverse optic modes of $SrGeO_3$. Solid lines, FPLAPW calculations; solid squares, reflectance IR measurements; hollow circles, absorbance IR (DAC) measurements. Pressures are given in GPa; frequencies in cm^{-1}.

Table 3. Experimental and theoretical optical frequencies and oscillator fit parameters. γ and ω parameters are in cm^{-1} units. $\varepsilon_\infty = 5.2$.

Assignment	$\Delta\varepsilon$	γ_{LO}	ω_{LO}	γ_{TO}	ω_{TO}	$\omega_{TO(LAPW)}$
'GeO_6'	100.5	19	203	39	121	123
O–Ge–O	07.1	10	492	7	220	234
Ge–O	01.2	55	773	33	620	616

An independent experimental estimate of the static dielectric constant for this sample was obtained by performing capacitance measurements at 100 Hz. The average of five measurements gave $\varepsilon(0) = 91 \pm 20$, in the same range as the value estimated from the fit to the IR reflectivity.

The pressure dependence of the highest-frequency TO mode (measured *in situ* by powder IR transmission in the diamond anvil cell) is shown in figure 4. At ambient pressure, the position of the transmission minimum lies about 20 cm^{-1} above the TO mode frequency, determined by reflectivity measurements (squares). The experimentally determined pressure shift of this mode is also compared with theoretical results in this figure. Theoretical estimates for the zone centre TO phonon frequencies as a function of volume were obtained using the frozen polar phonon procedure [38] within the LAPW framework. The LAPW calculations were performed using $RK_{max} = 8$, and 18 special k-points for the reciprocal space integration, yielding energies converged to $\sim$0.1 mH (milliHartree). The F_{1u} subblock of the dynamical matrix is constructed in a symmetry adapted basis by directly calculating total energy differences due to internal atomic displacements (within a $P4mm$ symmetry) relative to the ideal cubic structure ($Pm3m$). Harmonic force constants are obtained by a quadratic fit to the energy–displacement data. The six matrix elements correspond to

independent Sr, Ge, O_I and concerted Sr–Ge, Sr–O_I and Ge–O_I internal distortions, with the O_{II} positions fixed (O_I and O_{II} refer to axial and equatorial oxygens in an octahedral unit, respectively). Force constants, fitted over the range 50 $Å^3$ to 60 $Å^3$ (five data points in between), exhibited the expected linear dependence on the lattice parameter (the lattice parameter dependence was fitted to a quadratic form yielding the coefficients given in table 4). According to the 300 K equation of state, the corresponding pressure range for this variation of volume is approximately 20 GPa (compression) to −15 GPa (tension) (figure 4). The interpolation of the force constants over this range is expected to be good, and because of the near linearity of the force constant dependence on the lattice parameter, the extrapolation outside of this range is also expected to be valid. Diagonalization of the F_{1u} subblock yielded the volume dependent transverse optic frequencies plotted in figure 4.

Table 4. Quadratic fit coefficients of the force constant matrix elements to the cubic lattice parameter, a. Superscripts$^{(n)}$ denote the coefficients of the a^n terms.

		$k_{ij}^{(0)}$ (H a_0^{-1})	$k_{ij}^{(1)}$ (H a_0^{-2})	$k_{ij}^{(2)}$ (H a_0^{-3})
$i = j$	Sr	2.5169	−0.5881	0.0340
	Ge	11.8498	−2.9306	0.1810
	O_I	12.5479	−3.0067	0.1792
$i \neq j$	Sr–Ge	−1.4496	0.3620	−0.0232
	Sr–O_I	5.5583	−1.5238	0.1042
	Ge–O_I	−8.5918	2.0413	−0.1196

The calculated frequencies for the ambient pressure volume are in excellent agreement with the TO mode frequencies obtained from the IR spectra at room pressure (figure 4 and table 3). At ambient pressure all transverse optic modes are predicted to be positive, indicating dynamical stability against the F_{1u} infinitesimal atomic displacements. Analysis of atomic displacement patterns associated with the optic modes at ambient pressure (table 5) shows that the lowest-frequency calculated TO mode at 123 cm^{-1} involves primarily *out-of-phase* displacements of the Ge and Sr atoms. This assignment differs from that for the lowest-frequency IR mode in other non-transition-metal perovskites [31], but is supported by our work on the volume and composition dependence of the infrared modes in the $SrGeO_3$–$SrTiO_3$ perovskite series [13, 37].

Table 5. Calculated infrared-active TO phonon frequencies and normalized atomic displacement patterns at ambient pressure ($V_0 = 55$ $Å^3$).

ω (cm^{-1})	u_z(Sr)	u_z(Ge)	$u_z(O_I)$	$u_z(O_{II})$
123	0.68	−0.19	−0.25	−0.46
234	0.34	−0.75	0.01	0.40
616	0.01	0.22	−0.93	0.21

The calculated volume dependence of the TO frequencies at 300 K reveals soft-mode behaviour for the lowest-lying F_{1u} mode in the tensile regime, with onset near −9 GPa (58.6 $Å^3$). There is a slight upward curvature in the $\nu(P)$ dependence of the second-lowest-lying mode below ∼−2 GPa, indicating strong coupling between the modes at larger volumes leading to symmetry-avoided crossing. It has been suggested that the thermally activated ferroic-like behaviour in silicate perovskites, decompressed from their

high-pressure stability fields, is fundamentally responsible for the occurrence of metastable crystal-to-amorphous transitions observed in these materials [10, 11]. Our results from theoretical modelling of $SrGeO_3$ perovskite suggest that such behaviour is a common one in these materials.

The existence of the first-order Raman spectrum of $SrGeO_3$ perovskite along with the structure observed on the IR bands indicate some small distortion from cubic symmetry. We have explored the origin of this distortion theoretically. A common destabilization mechanism in cubic perovskite-like systems involves the cooperative rotation or tilting of the octahedral subunits. We performed a suite of calculations to allow for the *in-phase* rotations of the GeO_6 octahedra about the c axis (the cubic M-point instability). For small rotation angles this degree of freedom can be parametrized by a single structural parameter, u, which represents the magnitude of the tangential displacement of an equatorial anion in the rotation plane (see figure 5). A lower bound on the relaxation energy was obtained by calculating the static lattice energy for a small range of the u parameter (typically up to a few per cent of a lattice constant), but for a fixed volume. Relaxing the volume constraint for small rotations would lower the energy even more. In order to make the cell-doubled calculations tractable but accurate we used $RK_{max} \sim 8$. To allow for the change in nearest-neighbour separation on rotation the atomic sphere radii were reduced by 5% relative to their optimal values for the $Pm3m$ cell, and the plane-wave cutoff was increased to compensate for this effect. To check the accuracy of the calculated energies with these choices we re-evaluated the energy in the undistorted cubic setting and found agreement with our original value to within 0.2 mRyd.

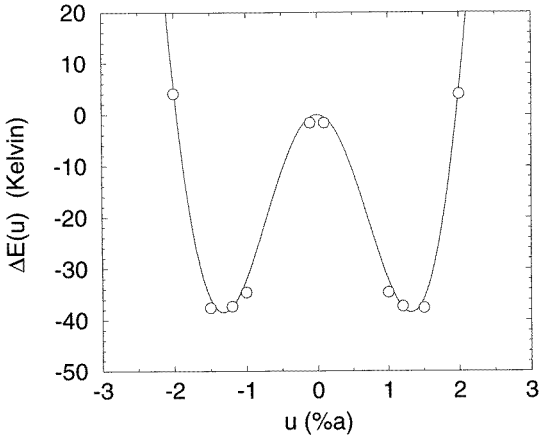

Figure 5. Ambient-pressure static crystal energy relative to the constrained cubic perovskite structure ($a = 10.17\ a_0$, $b = 7.20\ a_0$). The distortion parameter u is specified as a fraction (%) of the lattice parameter a. The solid line is a fit to a third-order polynomial in u. Energies are given in kelvin.

A plot of the distortion energy as a function of u is shown in figure 5. There is a small energy gain ($\sim$38 K; 3.3 meV per cubic formula unit) associated with the rotational distortion, consistent with the IR and Raman results. We estimate that a simultaneous volume relaxation would deepen the side-wells by no more than a factor of two. Using the non-empirical VIB model [18], which also predicts the occurrence of R- and M-point phonon soft modes, we calculated the energy of the constrained volume rotational energy lowering and the fully optimized energy of the relaxed $P4mm$-symmetry crystal. The static

lattice energy lowering obtained using this method was approximately 4.4 meV, ∼38% larger than for the LAPW result (figure 5).

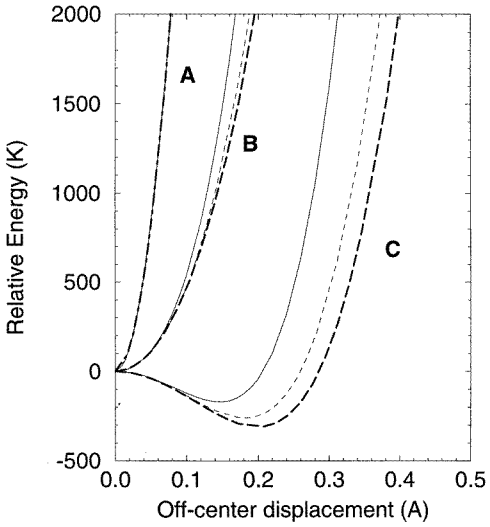

Figure 6. Energy associated with off-centre displacement of the Ge atom within an octahedral oxygen cage. Displacements along three lines emanating from the centre of the cage are shown: toward an octahedral corner, [100], solid line; to an octahedral edge, [110], dashed line, and toward an octahedral face centre, [111], bold dashed line. The sets of curves marked A, B and C correspond, respectively, to a linear cage expansion of 0, 4 and 6.8% (or equivalent pressures of 0, −14 and −20 GPa in the equivalent crystalline system).

In order to gain more insight into the origin of the cage mode instability we have examined the dependence of the internal energy surface of the GeO_6 octahedron on isotropic strain. To do so we employed a simple cluster model based on a parametric tight-binding scheme (the PM3 model). Full geometry optimization was performed on the charge-compensated cluster $Ge(OH)_6^{2-}$ to obtain a reference energy. An equilibrium Ge–O bond-length of 1.90 Å was obtained, which, perhaps fortuitously, corresponds exactly to the equilibrium Ge–O bond-length in the crystalline phase measured at ambient pressure. A similar calculation for the $Si(OH)_6^{2-}$ cluster, using the same basis set, yields $d(\text{Si–O}) = 1.80$ Å, which is very similar to the Si–O bond length 1.78 Å found in metastable cubic $CaSiO_3$. The effects of strain were explored by expanding all the Ge–O bonds and then displacing, for that fixed arrangement, the Ge position within the cage. The resulting energy surface is in general anisotropic, yielding a different displacement dependence along the [100], [110] and [111] directions. This anisotropy depends very sensitively on the local strain experienced by the cage, which is itself related to the macroscopic strain developed within the crystal. Our model results are shown in figure 6, which contains three sets of curves corresponding, respectively, to volume strains of 0, 12 and 20% (or pressures equivalent to 0, −14 and −20 GPa, assuming homogeneous deformation). As can be seen from the figure, the instability in the lowest-lying cage mode develops rapidly with increasing strain. The most significant reduction in the internal energy is for Ge^{4+} displacement in the [111] direction, followed by those associated with displacements along the [110] and [100] directions. These trends are consistent with earlier findings based on much more elaborate calculations for $BaTiO_3$ [38], and track the polar distortions described

previously for the cubic → tetragonal → orthorhombic para/ferroelectric phase transitions in perovskites [39]. Such large off-centre (hence intrinsically polar) displacements of the Ge^{4+} cations could well be viewed as the origin of the unusually high dielectric constant in the decompressed $SrGeO_3$ perovskite phase. In this respect, it is worth noting that $SrTiO_3$ could be considered as an 'expanded' version of the $SrGeO_3$ structure [12], harking back to the early interpretation of ferroelectric behaviour in perovskites proposed by Slater [40]. It is also of interest to note that the potential interplay between such local GeO_6 distortions, the ferroelectric zone centre mode softening and the zone boundary anti-ferroelastic instabilities makes this material an ideal candidate for observation of 'dirty' ferroelectric, or 'relaxator' behaviour, in an end-member, valence-satisfied perovskite phase [41].

Acknowledgments

We thank R Chamberlin for his support, useful suggestions and access to his laboratory for dielectric constant measurements. This work has been funded by the NSF under MRSEC award DMR 9121570. AG acknowledges a post-doctoral fellowship from the French Ministry of Foreign Affairs. GW acknowledges support from project grants CHE-9012249 and EAR-9105510.

References

[1] Liu L G 1974 *Geophys. Res. Lett.* **1** 277
[2] Liu L G 1975 *Geophys. Res. Lett.* **2** 417
[3] Durben D J and Wolf G H 1992 *Am. Mineral.* **77** 890
[4] Leinenweber K, Wang Y, Yagi T and Yusa H 1994 *Am. Mineral.* **79** 197
[5] Susaki J, Akimoto S and Yagi T 1982 *Programme and Abstracts, Seism. Soc. Japan* **1** 122
[6] Durben D J, Wolf G H and McMillan P F 1991 *Phys. Chem. Miner.* **18** 215
[7] Lu R and Hofmeister A M 1994 *Phys. Chem. Miner.* **21** 78
[8] Gasparik T, Wolf K and Smith C M 1994 *Am. Mineral.* **79** 1219
[9] Mao H K, Chen L C, Hemley R J, Jephcoat A P, Wu Y and Bassett W A 1989 *J. Geophys. Res.* **94** 17 889
[10] Hemmati M, Chizmeshya A, Wolf G H, Poole P H, Shao J and Angell A 1995 *Phys. Rev.* B **51** 14 841
[11] Chizmeshya A, Wolf G H and McMillan P F 1996 *Geophys. Res. Lett.* **23** 2725. An erratum is currently at press to correct a typographical error in table 3 of this letter. The actual displacement patterns of the LAPW F_{1u} modes in $CaSiO_3$ are in fact very similar to those reported here for $SrGeO_3$.
[12] Walker D, Carpenter M A and Hitch C M 1990 *Am. Mineral.* **75** 1020
[13] Grzechnik A, McMillan P F, Chamberlin R, Hubert H and Chizmeshya A 1997 *Eur. J. Solid State Inorg. Chem.* **34** 269
[14] Mao H K, Bell P M, Shaner J W and Heinberg D J 1978 *J. Appl. Phys.* **49** 3276
[15] Blaha P, Schwartz K, Dufek P and Augustyn R 1995 *WIEN95* Technical University of Vienna. Improved and updated Unix version of the original copyrighted WIEN code, P Blaha, K Schwartz, P Sorantin and S B Trickey 1990 *Comput. Phys. Commun.* **59** 399
[16] Kohn W and Sham L J 1965 *Phys. Rev.* **140** A1133
[17] Wolf G H and Bukowinski M 1987 *High-Pressure Research in Mineral Physics (Geophys. Monogr. Ser. 39)* ed M H Manghnani and Y Syono (Washington, DC: AGU) pp 313–31
[18] Chizmeshya A, Zimmermann F M, LaViolette R A and Wolf G H 1994 *Phys. Rev.* B **50** 15 559
[19] Sato Y and Akimoto S 1979 *High-Pressure Science and Technology, 6th AIRAPT Conf.* vol 2, ed K D Timmerhaus and M S Barber (Singapore: World Scientific) p 91
[20] Shimizu Y, Syono Y and Akimoto S 1970 *High Temp.–High Pressures* **2** 113
[21] Grzechnik A, Petuskey W and McMillan P F 1995 *Thermodynamics and Kinetics of Phase Transitions (Mater. Res. Soc. Symp. Proc. 398)* (Pittsburgh, PA: Materials Research Society) p 501
[22] Andrault D, Peryronneau J, Farges F and Itié J-P 1995 *Physica* B **208** 327
[23] Andrault D, Itié J-P and Farges F 1996 *Am. Mineral.* **81** 822
[24] Glazer A M 1972 *Acta Crystallogr.* B **28** 3384
[25] Lockwood D J and Torrie B H 1974 *J. Phys. C: Solid State Phys.* **7** 2729

[26] Alexandrov K S 1976 *Ferroelectrics* **14** 801
[27] Salje E 1976 *Acta Crystallogr.* A **32** 233
[28] Strobel K and Geick R 1979 *J. Phys. C: Solid State Phys.* **12** 3855
[29] Woodward P M 1997 *Acta Crystallogr.* B **53** 32
[30] Woodward P M 1997 *Acta Crystallogr.* B **53** 44
[31] Gervais F 1985 *Japan J. Appl. Phys.* **24** 198
[32] Taylor W and Murray A F 1979 *Solid State Commun.* **31** 937
[33] Perry C H, Fertel J H and McNelly T F 1967 *J. Chem. Phys.* **47** 1619
[34] Nilsen W G and Skinner J G 1968 *J. Chem. Phys.* **48** 2240
[35] Reissland J A 1973 *The Physics of Phonons* (London: Wiley)
[36] Servoin J L, Luspin Y and Gervais F 1980 *Phys. Rev.* B **22** 5501
[37] Grzechnik A, Hubert H, Petuskey W and McMillan P F 1997 *Integrated Ferroelectr.* **15** 191
[38] Cohen R E and Krakauer H 1990 *Phys. Rev.* B **42** 6416
[39] Verble J L, Gallego-Lluesma E and Porto S P S 1978 *J. Raman Spectrosc.* **70** 7
[40] Slater J C 1950 *Phys. Rev.* **78** 748
[41] Samara G A 1991 *Ferroelectrics* **117** 347